CrossMark

RESEARCH ARTICLE

Estimating the Instantaneous Drag–Wind Relationship for a Horizontally Homogeneous Canopy

Ying Pan[1] · Marcelo Chamecki[1] · Heidi M. Nepf[2]

Abstract The mean drag–wind relationship is usually investigated assuming that field data are representative of spatially-averaged metrics of statistically stationary flow within and above a horizontally homogeneous canopy. Even if these conditions are satisfied, large-eddy simulation (LES) data suggest two major issues in the analysis of observational data. Firstly, the streamwise mean pressure gradient is usually neglected in the analysis of data from terrestrial canopies, which compromises the estimates of mean canopy drag and provides misleading information for the dependence of local mean drag coefficients on local velocity scales. Secondly, no standard approach has been proposed to investigate the instantaneous drag–wind relationship, a critical component of canopy representation in LES. Here, a practical approach is proposed to fit the streamwise mean pressure gradient using observed profiles of the mean vertical momentum flux within the canopy. Inclusion of the fitted mean pressure gradient enables reliable estimates of the mean drag–wind relationship. LES data show that a local mean drag coefficient that characterizes the relationship between mean canopy drag and the velocity scale associated with total kinetic energy can be used to identify the dependence of the local instantaneous drag coefficient on instantaneous velocity. Iterative approaches are proposed to fit specific models of velocity-dependent instantaneous drag coefficients that represent the effects of viscous drag and the reconfiguration of flexible canopy elements. LES data are used to verify the assumptions and algorithms employed by these new approaches. The relationship between mean canopy drag and mean velocity, which is needed in models based on the Reynolds-averaged Navier-Stokes equations, is parametrized to account for both the dependence on velocity and the contribution from velocity variances. Finally, velocity-dependent drag coefficients lead to significant variations of the calculated displacement height and roughness length with wind speed.

✉ Marcelo Chamecki
   chamecki@psu.edu

[1] Department of Meteorology, Pennsylvania State University, University Park, PA 16802, USA

[2] Department of Civil and Environmental Engineering, Massachusetts Institute of Technology, Cambridge, MA 02139, USA

1 Introduction

Modelling the dynamic interactions between flow and vegetation is essential for reproducing the complex turbulent flow field within and above plant canopies. In order to bypass the difficulty of computing boundary conditions on the surfaces of individual canopy elements, spatial averaging over horizontal planes or "thin slabs" is applied to the Navier-Stokes equations. In the resulting equations, effects of vegetation on the flow appear as distributed form and viscous drag forces (Wilson and Shaw 1977). The distributed drag force depends on the leaf area density, the velocity, and the local drag coefficient. This framework has been used in a range of modelling approaches including one-dimensional first- and second-order closure (Wilson and Shaw 1977; Katul 1998; Pinard and Wilson 2001; Poggi et al. 2004a; Katul et al. 2011), Reynolds-averaged Navier–Stokes (RANS; Dupont et al. 2006) and large-eddy simulation (LES; Shaw and Schumann 1992; Su et al. 1998; Patton et al. 2003; Shaw and Patton 2003; Yue et al. 2007b; Dupont and Brunet 2008; Gavrilov et al. 2013; Pan et al. 2014a). Turbulence statistics predicted by these models are highly sensitive to the parametrization schemes employed for the local mean and instantaneous drag coefficients. While a constant drag coefficient model has been widely used, in reality the local drag coefficients tend to decrease with increasing local velocity due to the effects of viscous drag (Raupach and Thom 1981; Poggi et al. 2004b) and reconfiguration of flexible canopy elements (Alben et al. 2002; Gosselin et al. 2010; Luhar and Nepf 2011). For terrestrial and aquatic canopies, this dependence is commonly observed to follow a power law of the local characteristic velocity scales with an exponent between zero and $-4/3$ (Vogel 1984; Gaylord et al. 1994; Harder et al. 2004; Albayrak et al. 2012; Queck et al. 2012; Pan et al. 2014a). For natural canopies in which simple bending is observed (e.g., seagrasses and wheat), both measurement and theory suggest a power-law exponent between $-2/3$ and -1 (Pan et al. 2014b).

Unlike the simple bending regime noted above, analytical models for the mean and instantaneous drag coefficients cannot be obtained from first principles for more complex canopies, and field data must be used to suggest empirical models for the drag coefficients. Traditionally, the mean drag coefficients are estimated using vertically distributed single-point measurements of instantaneous velocity time series (e.g., Pinard and Wilson 2001). This traditional approach assumes that data are representative of spatially-averaged metrics of statistically stationary flow within and above a horizontally homogeneous canopy. Even if these conditions are satisfied, two major issues remain in the analysis of observational data. Firstly, the streamwise mean pressure gradient is typically neglected for terrestrial canopies, mostly due to the difficulty in estimating it from measurements (e.g., Cescatti and Marcolla 2004; Queck et al. 2012). Secondly, despite the expected dependence of the mean local drag coefficients on the local velocity scales, no standard approach has been proposed to estimate the instantaneous drag coefficients that correlate with instantaneous velocities.

The instantaneous drag–wind relationship characterized by the instantaneous drag coefficient is a critical component of canopy representation in LES. Canopy-resolving LES models using a constant drag coefficient (e.g., Shaw and Schumann 1992; Su et al. 1998; Patton et al. 2003; Yue et al. 2007b; Dupont and Brunet 2008; Gavrilov et al. 2013) can reproduce profiles of mean velocity, mean vertical momentum flux and components of turbulent kinetic energy (TKE) measured in the field. However, the skewness of streamwise and vertical velocity fluctuations are underestimated by more than 50 % with respect to the measurements. Strong

events, evaluated using quadrant analysis, are also not well reproduced (Yue et al. 2007a). Pan et al. (2014a, b) reported that using an instantaneous drag coefficient that followed a power law of instantaneous velocity with an exponent between $-2/3$ and -1 significantly improved the prediction of velocity skewness and the prediction of the fraction of vertical momentum flux carried by strong events. As the power-law exponent became more negative, the peak in the skewness of the streamwise velocity component increased in magnitude and its location moved downwards, corresponding to greater magnitude and penetration of strong downward events within the canopy (Pan et al. 2014b). Given the sensitivity of high-order turbulence statistics to the choice of the power-law exponent, an accurate model of the instantaneous drag coefficient is critical for LES models to reproduce the structure of turbulence as well as the transport of scalars within and above the plant canopy.

Reliable estimates of the drag–wind relationship are important not only for canopy-resolving models, but also for the parametrization of the rough-wall boundary condition used by models that do not resolve the canopy layer. Physically, the zero-plane displacement (displacement height), d_0, is defined for a virtual wall boundary layer to reproduce flow statistics above the canopy roughness sublayer. The definition based on the mean shear stress links the displacement height to the vertical distribution of the mean canopy drag within the canopy (Thom 1971; Jackson 1981). Consequently the variability in the drag–wind relationship is expected to cause variability in the displacement height that directly affects the flux-gradient relationship above the canopy. Improving estimates of the displacement height reduces errors in estimating the mixing length as well as the aerodynamic roughness length, z_0, an essential parameter that characterizes the link between the mean shear stress at the canopy top and the mean wind speed above the canopy roughness sublayer.

The objective of this work is to bridge the traditional estimates of the mean drag–wind relationship with the target estimates of the instantaneous drag–wind relationship. Firstly, a practical approach is proposed to estimate the streamwise mean pressure gradient, which enables reliable investigation of the mean drag–wind relationship. Secondly, iterative approaches are proposed to bridge the models for mean and instantaneous local drag coefficient. These new approaches require no additional data than are available in the usual approaches, (i.e., vertically distributed instantaneous velocity time series). In practice, instrumental errors and data representativeness issues (due to non-stationarity, finite field size, and the true spatial distribution of canopy elements) may induce additional variability in the mean and instantaneous drag–wind relationships. In order to bypass these concerns, the new approaches are evaluated using LES data of statistically stationary flow within and above a horizontally homogeneous model canopy (Sect. 3). Specifically, the LES runs are conducted with postulated models of the instantaneous drag coefficient, and the velocity frelds are used to retrieve mean and instantaneous local drag coefficients. The evaluation is performed for high and low wind speeds and three types of instantaneous drag coefficient: (i) a constant; (ii) a power-law function of instantaneous velocity; and (iii) a capped power-law function of instantaneous velocity. The physical rationale for these drag coefficient models is explained in Sect. 2.3. The advantage of using LES here is that the "true" drag–wind relationship is known and the effects of various assumptions made during data analysis on the final estimates of the drag coefficient can be assessed. The implications for the models of the mean local drag coefficient and the displacement height are discussed in Sect. 4. The major findings and practical limitations are summarized in Sect. 5.

2 Methodology for Estimating the Local Drag–Wind Relationships

In Sect. 2.1, we first review the origin of the mean canopy drag from the application of a horizontal averaging operator to the Navier-Stokes equation. Then we review various models for the mean canopy drag, the physical rationale for the mean and instantaneous local drag coefficients, and the traditional approaches to investigate the mean drag–wind relationship. In Sect. 2.2, a practical approach to estimating the streamwise mean pressure gradient from typical measurements in terrestrial canopies is described. In Sect. 2.3, approaches are proposed to identify the functional form for the instantaneous drag coefficients, and then to fit parameters for the specific functional forms.

2.1 Models of Mean Canopy Drag and Traditional Estimates of Local Drag Coefficients

The Boussinesq approximation of the Navier-Stokes equation in a rotating frame of reference is,

$$\frac{\partial \boldsymbol{u}}{\partial t} + \nabla \cdot (\boldsymbol{u}\boldsymbol{u}) = -\frac{1}{\rho_0}\nabla p + \frac{\rho}{\rho_0}\boldsymbol{g} + \nu\nabla^2\boldsymbol{u} - 2\boldsymbol{\Omega} \times \boldsymbol{u}, \tag{1}$$

where $\boldsymbol{u}$ is the instantaneous fluid velocity, ν is the kinematic viscosity of the fluid, $\boldsymbol{g}$ is the effective acceleration due to gravity on Earth, and $\boldsymbol{\Omega}$ is the angular velocity of Earth with respect to its own axis. Variables p and ρ are the perturbations of pressure and density of the fluid with respect to their base state, p_0 and ρ_0, respectively. The statistics of the flow can be investigated using three types of averaging operators: (i) $\langle \Phi \rangle$, a horizontal average over a plane large enough to eliminate variations due to both the canopy structure and the largest length scales of turbulence (discussed in Raupach and Shaw 1982), (ii) $\overline{\Phi}$, a single-point time average over an interval large enough to eliminate variations due to the largest time scales of turbulence, and (iii) $\widehat{\Phi}$, a horizontal average over a plane large enough to eliminate variations due to the canopy structure, and at the same time small enough to preserve large scales of turbulence. Wilson and Shaw (1977) asserted that $\langle \Phi \rangle = \overline{\widehat{\Phi}} = \widehat{\overline{\Phi}}$. Applying the averaging operator $\langle \Phi \rangle$ to (1), we obtain

$$\frac{\partial \langle \boldsymbol{u} \rangle}{\partial t} + \nabla \cdot \langle \boldsymbol{u}\boldsymbol{u} \rangle = -\frac{1}{\rho_0}\nabla\langle p \rangle + \frac{\langle \rho \rangle}{\rho_0}\boldsymbol{g} + \nu\nabla^2\langle \boldsymbol{u} \rangle - 2\boldsymbol{\Omega} \times \langle \boldsymbol{u} \rangle - \frac{1}{\rho_0}\langle \nabla p'' \rangle + \nu\langle \nabla^2 \boldsymbol{u}'' \rangle, \tag{2}$$

where $\Phi'' = \Phi - \langle \Phi \rangle$ is the departure from the average value, $\langle \Phi \rangle$. The last two terms on the right-hand side of (2) arise through non-commutativity of horizontal averaging and spatial derivatives. Physically they represent the form and viscous drag forces imposed by the canopy.

The mean canopy drag represents a net surface force acting on the interface between canopy elements and the flow, and depends on the leaf area density and the velocity. Using the mean velocity ($\langle \boldsymbol{u} \rangle$) as a characteristic flow velocity, we obtain a model for the mean canopy drag,

$$\langle \boldsymbol{f} \rangle = -\langle C_{\mathrm{d}} \rangle a |\langle \boldsymbol{u} \rangle| \langle \boldsymbol{u} \rangle, \tag{3}$$

where a is the leaf area density. The local mean drag coefficient, $\langle C_{\mathrm{d}} \rangle$, which characterizes the relationship between mean canopy drag and mean velocity, has three major sources of variability. Firstly, the viscous drag does not increase with the square of mean velocity, introducing a dependence of $\langle C_{\mathrm{d}} \rangle$ on Reynolds number (Schlichting and Gersten 2000). This dependence of $\langle C_{\mathrm{d}} \rangle$ on Reynolds number varies with the relative importance of form and viscous drag forces (Raupach and Thom 1981), which is difficult to predict due to the

complexity associated with the interference of wakes behind various canopy elements (Poggi et al. 2004b). Secondly, if canopy elements are flexible, then reconfiguration (bending and streamlining of canopy elements) reduces the increase of drag force with velocity, introducing a dependence of $\langle C_d \rangle$ on the Cauchy number that measures the relative importance of fluid forces and plant rigidity (Alben et al. 2002; Gosselin et al. 2010; Luhar and Nepf 2011). Note that the dependence of $\langle C_d \rangle$ on both Reynolds and Cauchy numbers can be combined into a dependence on velocity. Thirdly, the work done by the canopy drag is expected to dissipate the total kinetic energy of the flow, whereas only the mean velocity directly appears on the right-hand side of (3). Therefore $\langle C_d \rangle$ must contain the variability associated with TKE and dispersive kinetic energy (DKE), as confirmed by direct numerical simulation (DNS) of a staggered arrangement of rigid cubes (Santiago et al. 2008).

Alternatively, the model of the mean canopy drag can be modified to account for the dissipation of TKE and DKE explicitly,

$$\langle \boldsymbol{f} \rangle = -\langle C_d \rangle_{\text{mod}} a \langle |\boldsymbol{u}|\boldsymbol{u} \rangle, \tag{4}$$

where the modified mean drag coefficient ($\langle C_d \rangle_{\text{mod}}$) characterizes the relationship between mean canopy drag and the velocity scale associated with total kinetic energy ($U = \langle |\boldsymbol{u}|\boldsymbol{u} \rangle^{1/2}$). Although single-point measurements are not always representative of spatially-averaged metrics of the flow, field data suggest that the dependence of $\langle C_d \rangle_{\text{mod}}$ on U is clearer and less scattered than the dependence of $\langle C_d \rangle$ on $\langle \boldsymbol{u} \rangle$ (Cescatti and Marcolla 2004; Queck et al. 2012).

The dependence of local mean drag coefficients on local velocity scales reflects the dependence of the instantaneous local drag coefficient, C_d, on the instantaneous velocity. Correspondingly, the model of the mean canopy drag is modified as,

$$\langle \boldsymbol{f} \rangle = -\langle C_d a |\boldsymbol{u}|\boldsymbol{u} \rangle. \tag{5}$$

Modelling the instantaneous drag–wind relationship is a common practice used in LES studies, while the instantaneous drag–wind relationship can significantly depart from the mean drag–wind relationship (see Pan et al. 2014a, Appendix B).

Deriving analytical models for the mean and instantaneous local drag coefficients from first principles is not trivial. Traditionally, vertically distributed single-point measurements of instantaneous velocity time series were used to investigate the mean drag–wind relationship (e.g., Cescatti and Marcolla 2004; Queck et al. 2012). This traditional approach assumes that data are representative of spatially-averaged metrics of statistically stationary flow within and above a horizontally homogeneous canopy (Pinard and Wilson 2001). With these conditions, (2) is simplified as,

$$\frac{\partial}{\partial z} \langle w''\boldsymbol{u}'' \rangle = -\frac{1}{\rho_0} \nabla \langle p \rangle + \frac{\langle \rho \rangle}{\rho_0} \boldsymbol{g} + \langle \boldsymbol{f} \rangle, \tag{6}$$

noting that the Coriolis and viscous forces of the mean flow ($-2\boldsymbol{\Omega} \times \langle \boldsymbol{u} \rangle$ and $\nu \nabla^2 \langle \boldsymbol{u} \rangle$) are neglected by assuming large Rossby and Reynolds numbers. The streamwise component of the mean canopy drag,

$$\langle f_x \rangle = \frac{\partial \langle u''w'' \rangle}{\partial z} + \frac{1}{\rho_0} \frac{\partial \langle p \rangle}{\partial x}, \tag{7}$$

is combined with (3) and (4) to provide estimates for the local mean drag coefficient. Typically, the streamwise mean pressure gradient is not measured directly. It can be shown from the vertical component of (6) that the streamwise mean pressure gradient is negative, height-

independent, and balances the divergence of mean shear stress above the canopy,

$$\frac{1}{\rho_0}\frac{\partial\langle p\rangle}{\partial x} = -\left[\frac{\partial\langle u''w''\rangle}{\partial z}\right]_{z/h>1}, \tag{8}$$

where h is the canopy height. This approach provides good estimates of the streamwise mean pressure gradient for submerged canopies in open channels (e.g., Ghisalberti and Nepf 2004; Poggi et al. 2004a), but it is impractical for field experiments over terrestrial canopies. Above a terrestrial canopy the vertical variation of $\langle u''w''\rangle$ is small compared with the magnitude of $\langle u''w''\rangle$. An uncertainty of 5 % in the estimated $\langle u''w''\rangle$ can induce an error of 100 % in estimating its vertical gradient that balances the streamwise mean pressure gradient. In field studies for terrestrial canopies, the streamwise mean pressure gradient in (7) is usually neglected (e.g., Pinard and Wilson 2001; Cescatti and Marcolla 2004; Queck et al. 2012). The resulting estimates of the mean drag coefficient describe the relationship between the divergence of mean shear stress and the local velocity scale, which can be significantly different from the drag–wind relationship. Specifically, inserting (4) into (7) yields,

$$\langle C_d\rangle_{\mathrm{mod}} = \langle C_d\rangle^\star_{\mathrm{mod}} - \gamma\left[\frac{1}{\rho_0}\frac{\partial\langle p\rangle}{\partial x}\right], \tag{9}$$

where $\gamma=1/\left(a\langle|\boldsymbol{u}|u\rangle\right)=1/\left(aU^2\right)$. The traditional estimator, $\langle C_d\rangle^\star_{\mathrm{mod}}=-\gamma\left(\partial\langle u''w''\rangle/\partial z\right)$, only reproduces the modified mean drag coefficient ($\langle C_d\rangle_{\mathrm{mod}}$) when the streamwise mean pressure gradient is negligible compared with the divergence of the mean shear stress ($[(1/\rho_0)(\partial\langle p\rangle/\partial x)]/[\partial\langle u''w''\rangle/\partial z] \ll 1$). In general, the traditional estimator underestimates the modified mean drag coefficient (i.e., $\langle C_d\rangle^\star_{\mathrm{mod}} < \langle C_d\rangle_{\mathrm{mod}}$), and the difference between $\langle C_d\rangle^\star_{\mathrm{mod}}$ and $\langle C_d\rangle_{\mathrm{mod}}$ varies with the local velocity scale (U). In extreme situations, values of $\langle C_d\rangle^\star_{\mathrm{mod}}$ can be negative, and the corresponding drag–wind relationship is physically unrealistic. In Sect. 2.2, a practical approach is proposed to estimated the streamwise mean pressure gradient using the profile of mean vertical momentum flux within the canopy.

2.2 A Practical Approach to Estimating the Streamwise Mean Pressure Gradient

Equation 9 suggests that if $\langle C_d\rangle_{\mathrm{mod}}$ is a constant, then $\langle C_d\rangle^\star_{\mathrm{mod}}$ decreases linearly with γ. The negative, height-independent streamwise mean pressure gradient is the slope of this linear relationship, which can be obtained using a least square fitting,

$$\left[\frac{1}{\rho_0}\frac{\partial\langle p\rangle}{\partial x}\right]^{\mathrm{fit}} = \frac{N^{\mathrm{fit}}\Sigma\langle C_d\rangle^\star_{\mathrm{mod}}\gamma - \Sigma\gamma\,\Sigma\langle C_d\rangle^\star_{\mathrm{mod}}}{N^{\mathrm{fit}}\Sigma\gamma^2 - \Sigma\gamma\,\Sigma\gamma}, \tag{10}$$

where N^{fit} is the number of samples.

In general, $\langle C_d\rangle_{\mathrm{mod}}$ is not constant, but decreases with increasing velocity due to effects of viscous drag (Raupach and Thom 1981; Schlichting and Gersten 2000; Poggi et al. 2004b) and reconfiguration of flexible canopy elements (Alben et al. 2002; Gosselin et al. 2010; Luhar and Nepf 2011). Empirical estimates of $\langle C_d\rangle$ and $\langle C_d\rangle_{\mathrm{mod}}$ usually show a power-law dependence on their characteristic velocity scales with an exponent between 0 and $-4/3$ (Thom 1971; Vogel 1984; Gaylord et al. 1994; Harder et al. 2004; Queck et al. 2012). The variation of $\langle C_d\rangle^\star_{\mathrm{mod}}$ with height can be assessed qualitatively based on empirical profiles of mean vertical momentum flux ($\langle u''w''\rangle$), the velocity scale associated with the total kinetic energy (U), and the leaf area density (a) (e.g., profiles for maize canopies shown in Fig. 1). In the upper canopy (above the *horizontal dotted line* in Fig. 1a), the divergence of the mean shear stress (i.e., the slope of the profile of the mean vertical momentum flux) is sufficiently
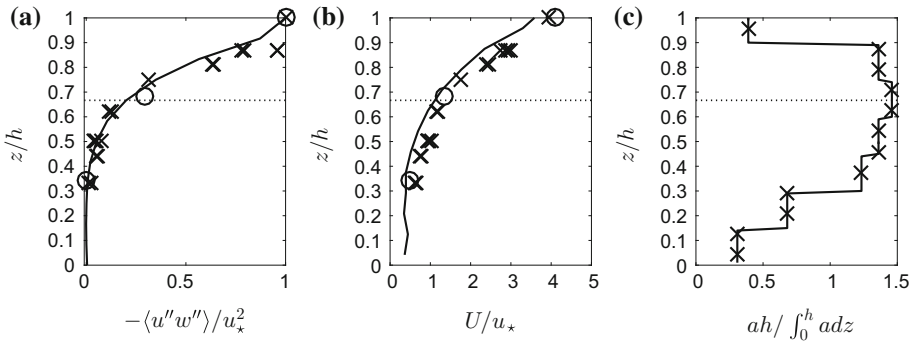
Fig. 1 Profiles of **a** normalized mean vertical momentum flux $(-\langle u''w''\rangle/u_\star^2)$, **b** normalized velocity scale associated with normalized total kinetic energy $(U/u_\star)$, and **c** normalized leaf area density $(ah/\int_0^h a\,dz)$ for maize canopies. *Crosses* in **a** and **b** as well as the *solid line* in **c** represent measurements obtained by Wilson et al. (1982), where the canopy height (h) is 2.21 m, and the friction velocity ($u_\star$) ranges from 0.4 to 0.8 m s^{-1}. Note that we took flow statistics from Wilson (1988), and consequently the velocity scale associated with total kinetic energy was calculated using the approximation, $U \approx \left[\langle u\rangle^2 + \langle u''w''\rangle + (1/2)\langle v''v''\rangle + (1/2)\langle w''w''\rangle\right]^{1/2}$. *Circles* in **a** and **b** represent measurements obtained by Gleicher et al. (2014), where $h = 2.1$ m, and $u_\star = 0.51$ m s^{-1}. *Solid lines* in **a** and **b** represent LES results obtained using an instantaneous drag coefficient model, $C_d = \min\left[(|\tilde{u}|/A)^B, C_{d,\max}\right]$, where $C_{d,\max} = 0.8$, $A = 0.38$ m s^{-1}, and $B = -1$. Among the five models for C_d described in Sect. 3.1, this model with $B = -1$ provides the best overall reproduction of first- to third-order turbulence statistics and the momentum flux carried by quadrant events measured by Gleicher et al. (2014) (see details from Pan et al. 2014a, b). *Crosses* in **c** indicate values of leaf area density specified on LES grids. The *horizontal dotted lines* at $z/h = 2/3$ represent an empirical division between upper and lower canopy regions. The slopes of the profiles of $\langle u''w''\rangle$ and U are much sharper in the upper canopy than in the lower canopy. The profile of the leaf area density also peaks around the division of the upper and lower canopy regions

large for the streamwise mean pressure gradient to be negligible in the force balance (7), and therefore $\langle C_d\rangle^\star_{\text{mod}} \approx \langle C_d\rangle_{\text{mod}}$, both of which decrease with increasing velocity magnitude. Because the characteristic velocity scale ($U = \langle|\boldsymbol{u}|u\rangle^{1/2}$) increases with height (see Fig. 1b), $\langle C_d\rangle^\star_{\text{mod}}$ decreases with height.

In the lower canopy, the divergence of mean shear stress becomes much smaller than that in the upper canopy (comparing the slope of the profile below and above the *horizontal dotted line* in Fig. 1a), and therefore the streamwise mean pressure gradient becomes important in the force balance (7). Meanwhile, the variability in the velocity scale associated with the total kinetic energy (U) in the lower canopy is also much smaller than that in the upper canopy (comparing the profile below and above the *horizontal dotted line* in Fig. 1b). Therefore the modified mean drag coefficient ($\langle C_d\rangle_{\text{mod}}$), which depends on U, only varies slightly with height. For terrestrial canopies, the leaf area density (a) typically increases with height in the lower canopy (see Fig. 1c for a maize canopy and Fig. 2 in Shaw and Schumann (1992) for a forest canopy). The combination of the small variability in U and the increase of leaf area density with height leads to a decrease of γ with height. The combination of the small variability in $\langle C_d\rangle_{\text{mod}}$ and the decrease of γ with height leads to an increase of $\langle C_d\rangle^\star_{\text{mod}}$ with height. In summary, for the general case where $\langle C_d\rangle_{\text{mod}}$ decreases with increasing velocity, $\langle C_d\rangle^\star_{\text{mod}}$ is expected to exhibit a local maximum within the canopy, which separates the canopy into upper and lower regions. Applying (10) to values of $\langle C_d\rangle^\star_{\text{mod}}$ and γ below the location of the maximum $\langle C_d\rangle^\star_{\text{mod}}$ provides estimates of the streamwise mean pressure gradient. Note that a local maximum usually exists in the profile of U in the lower canopy region (i.e., at

$z/h = 0.15$ in Fig. 1b). In some forest canopies, the vertical gradients of U may be sharp except for within the vicinity of its local maximum (e.g., according to the nocturnal mean wind-speed profile in Baldocchi and Meyers 1998). In this situation, the fitting approach (10) should be applied to the region below the local maximum of $\langle C_d \rangle^{\star}_{\mathrm{mod}}$ and with small vertical gradients of U.

2.3 Approaches to Estimate the Instantaneous Drag–Wind Relationship

Quantifying the correlation between instantaneous drag coefficients and velocities assumes that a single analytical model, $C_d = C_d(\boldsymbol{u})$, is applicable to multiple layers within the canopy. Three specific functional forms are postulated. First, C_d is a constant, an assumption used in many LES studies (e.g., Shaw and Schumann 1992; Su et al. 1998; Patton et al. 2003; Yue et al. 2007b; Dupont and Brunet 2008; Gavrilov et al. 2013). DNS results suggest that a constant instantaneous drag coefficient is a good model for rigid canopies (Santiago et al. 2008). Second, C_d decreases as a power-law function of the magnitude of the instantaneous velocity ($|\boldsymbol{u}|$), which accounts for the effects of viscous drag and reconfiguration,

$$C_d = (|\boldsymbol{u}|/A)^B, \tag{11}$$

where A is a velocity scale, B is a negative power-law exponent. Third, C_d is a constant ($C_{d,\max}$) at low velocity, but decreases as a power-law function of $|\boldsymbol{u}|$ above a critical velocity. This model accounts for a minimum velocity needed to initiate reconfiguration,

$$C_d = \min\left[(|\boldsymbol{u}|/A)^B, C_{d,\max}\right]. \tag{12}$$

For $B = 0$, Eqs. (11) and (12) reduce to a constant.

Estimating the instantaneous drag–wind relationship requires iterative approaches for pre-determined functional forms of the instantaneous drag coefficients. LES results suggest that $\langle C_d \rangle_{\mathrm{mod}} = \langle C_d \rangle_{\mathrm{mod}}(U)$ and $C_d = C_d(\boldsymbol{u})$ share the same functional form (see Sect. 3.2). For the constant instantaneous drag coefficient case, $C_d = \langle C_d \rangle_{\mathrm{mod}}$. For (3) and (4), estimates of $\langle C_d \rangle_{\mathrm{mod}}$ show a power law and a capped power law of U, and are used as the initial guess ($C_{d,0}$) for iterative approaches proposed in Sects. 2.3.1 and 2.3.2.

2.3.1 A Power-Law Drag Coefficient Model

Inserting (11) into (5) yields,

$$\langle f_x \rangle = -a\langle |\boldsymbol{u}|^{1+B}u \rangle/A^B, \tag{13}$$

where parameters A and B can be solved iteratively. Let N be the number of layers used to estimate the model of drag coefficient, and N_k be the number of velocity records taken at the kth layer. Parameters α_n and β_n are solved for using the system of a weighted least-square fitting,

$$\sum_{k=1}^{N} \sum_{i=1}^{N_k} W_{k,i} \left[y_{k,i} - (\beta_n x_{k,i} + \alpha_n) \right]^2 = \min\left(\sum_{k=1}^{N} \sum_{i=1}^{N_k} W_{k,i} \left[y_{k,i} - (\beta x_{k,i} + \alpha) \right]^2 \right), \tag{14}$$

where n is the index of iteration, $y_{k,i} = [\ln(C_{d,n-1})]_{k,i}$, $x_{k,i} = [\ln(|\boldsymbol{u}|)]_{k,i}$, and $W_{k,i} = [|\boldsymbol{u}|^2]_{k,i}$. Then we obtain $A_n = \exp(-\alpha_n/\beta_n)$ and $B_n = \beta_n$.

Putting the value of B_n into (13) yields,

$$A_{n+1/2} = \left[\frac{\langle f_x \rangle}{-a\langle |\boldsymbol{u}|^{1+B_n}u \rangle} \right]^{-1/B_n}. \tag{15}$$

Then we obtain a set of drag coefficients for the next iteration,

$$C_{d,n} = (|\boldsymbol{u}|/A_{n+1/2})^{B_n}. \tag{16}$$

If values of $A_{n+1/2}$ for various layers are different, then repeating (14–16) yields an updated power-law exponent, B_{n+1}, different from B_n. We repeat (14–16) until the criterion $|(B_{n+1} - B_n)/B_n| < 0.01$ is satisfied.

2.3.2 A Capped Power-Law Drag Coefficient Model

The constant instantaneous drag coefficient in the low-velocity regime, $C_{d,max}$, is obtained as the maximum of $C_{d,0} = \langle C_d \rangle_{mod}$. Then the critical velocity to initiate the reconfiguration is,

$$U_{c,n} = C_{d,max}^{1/B_n} A_n. \tag{17}$$

Let N_k be the number of velocity records at the kth layer and $N_{k,n}$ be the number of records $|\boldsymbol{u}| > U_{c,n}$. For this case, (14) is modified by replacing N_k with $N_{k,n}$ so that the weighted least-square fitting is only applied to drag coefficients estimated for $|\boldsymbol{u}| > U_{c,n}$. Correspondingly the expression of $A_{n+1/2}$ is revised as

$$A_{n+1/2} = \left[\frac{-\frac{N_k \langle f_x \rangle}{a} - \Sigma_{j=1}^{N_k - N_{k,n}} \left[C_{d,max} |\boldsymbol{u}| u \right]_j}{\Sigma_{i=1}^{N_{k,n}} \left[|\boldsymbol{u}|^{1+B_n} u \right]_i} \right]^{-1/B_n}. \tag{18}$$

We repeat (17–18) until the criterion $|(B_{n+1} - B_n)/B_n| < 0.01$ is satisfied.

3 Validation Against LES Data

Here the iterative approaches for estimating C_d presented in Sects. 2.2 and 2.3 are evaluated against previously validated LES data, which provide spatially-averaged metrics of statistically stationary flow within and above a horizontally homogeneous model canopy. The appropriateness of assumptions and the accuracy of the algorithms are tested by comparing the estimated models of the instantaneous drag coefficient with those imposed in the LES. In addition, guidelines are provided for data-analysis procedures when the streamwise mean pressure gradient is unavailable.

3.1 Description of LES Data

The LES model employed here is described in detail by Pan et al. (2014a), where the effects of canopy on the flow are represented as a distributed drag. The three-dimensional filtered momentum equation is solved using a fully de-aliased pseudo-spectral approach in the horizontal directions and a second-order centered finite-difference approach in the vertical direction. We use $\widetilde{\Phi}$ to represent the LES resolved fields, with the implicit assumption that the spatial filtering is carried over a plane large enough to eliminate variances due to the canopy structure and a vertical interval fine enough to resolve the canopy-shear-layer eddies. Applying this spatial filtering to (1) yields,

$$\frac{\partial \widetilde{\boldsymbol{u}}}{\partial t} + \boldsymbol{\nabla} \cdot (\widetilde{\boldsymbol{u}\boldsymbol{u}}) = -\frac{1}{\rho_0} \boldsymbol{\nabla} \widetilde{p} + \frac{\widetilde{\rho}}{\rho_0} \boldsymbol{g} + \nu \nabla^2 \widetilde{\boldsymbol{u}} - 2\boldsymbol{\Omega} \times \widetilde{\boldsymbol{u}} - \frac{1}{\rho} \widetilde{\boldsymbol{\nabla} p'} + \nu \widetilde{\nabla^2 \boldsymbol{u}}. \tag{19}$$

where $\Phi' = \Phi - \widetilde{\Phi}$ is the departure from the filtered value. Note that the LES filter ($\widetilde{\Phi}$) is also a spatial average. If the filter width in the LES is much larger than the scale of individual canopy elements, then $\widetilde{\Phi}$ can be interpreted as the horizontal average that eliminates the details of canopy structure ($\widehat{\Phi}$). The second term on the left-hand side of (19) can be split into two parts, $\nabla \cdot (\widetilde{u}\widetilde{u})$ and the divergence of SGS momentum flux, $\nabla \cdot \boldsymbol{\tau}$. The deviatoric part of $\boldsymbol{\tau}$ is parametrized using the Lagrangian scale-dependent dynamic Smagorinsky SGS model (Bou-Zeid et al. 2005). The non-deviatoric part of $\boldsymbol{\tau}$ is combined with $\widetilde{p}$ to form an effective pressure, which is then solved using the pressure Poisson equation. The viscous term, $\nu\nabla^2\widetilde{u}$, is neglected due to large Reynolds number associated with resolved velocity and grid spacing. The last two terms on the right-hand side of (19) represent form and viscous drag forces exerted by canopy elements within the grid. They are combined as a resolved canopy drag (Shaw and Schumann 1992),

$$\widetilde{f} = -C_\mathrm{d}a|\widetilde{u}|\widetilde{u}. \tag{20}$$

In this work, LES runs were conducted for a horizontally homogeneous model canopy; the canopy height ($h = 2.1$ m), the leaf area index ($LAI = 3.3$) and the leaf area density (a) were obtained from cornfield experimental data reported by Gleicher et al. (2014) and Wilson et al. (1982) (reviewed by Pan et al. 2014a). The simulation domain is a box with $L_x \times L_y \times L_z = 20h \times 20h \times 10h$, discretized using $84 \times 84 \times 120$ grid points. The model canopy occupies the entire horizontal domain and the lowest 12 vertical grids. The flow was driven by an imposed streamwise mean pressure gradient, while buoyancy and Coriolis forces were not considered. The horizontal, upper and lower boundary conditions were periodic, no-stress and solid rough wall, respectively. Simulation results are not sensitive to parameters specified for the wall model and the performance of the SGS model at the lowest levels because the model canopy is so dense that little momentum penetrates to the ground beneath the canopy. A total of ten runs were conducted for strong and weak wind cases ($u_\star = 0.51$ and $0.1\,\mathrm{m\,s}^{-1}$, respectively) using five models for the instantaneous drag coefficient classified into three functional forms introduced in Sect. 2.3: (i) C_d is a constant, (ii) C_d is a power-law function of instantaneous resolved velocity, and (iii) C_d is a capped power-law function of instantaneous resolved velocity. The mathematical expressions and values of parameters are listed in Table 1. Postulating the functional form of $C_\mathrm{d} = C_\mathrm{d}(|\widetilde{u}|)$ and the value of the power-law exponent (B), Pan et al. (2014a, b) fitted the other parameters in the model of C_d to reproduce the profile of the mean vertical momentum flux within a maize canopy observed by Gleicher et al. (2014), when $u_\star = 0.51\,\mathrm{m\,s}^{-1}$. Note that a constant C_d is equivalent to $B = 0$, and three values of B were postulated for C_d modelled as a capped power-law function of instantaneous resolved velocity. All fives runs for the strong wind case reproduced first- and second-order turbulence statistics within and above the maize canopy, while the model with $B = -1$ yielded the best reproduction of momentum flux carried by quadrant events and the skewness of streamwise and vertical velocity fluctuations (Pan et al. 2014a, b). Nevertheless, the field experiment of Gleicher et al. (2014) only provides single-point measurements at three heights within the maize canopy, a vertical resolution too coarse to retrieve the model of C_d from the profile of the mean vertical momentum flux.

Each LES run was conducted for 1.5 h using a timestep of 0.006 s. The analysis of data uses results from the last hour of each LES case study, when the turbulence has reached a statistically steady state. Specifically, we use the instantaneous field of resolved velocity output every 6 s, providing $N_k = 600 \times 84 \times 84$ records for each layer during a 1-h time period. Drag coefficient models were estimated from LES data with and without the inclusion of the streamwise mean pressure gradient. For the purpose of distinction, symbols without superscript represent results for which the streamwise mean pressure gradient was obtained

Table 1 Models of drag coefficient imposed into LES and values of corresponding parameters

Case	Model	A (m s^{-1})	B	$C_{d,max}$
(i)	$C_d = 0.25$	–	–	–
(ii)	$C_d = (|\widetilde{\boldsymbol{u}}|/A)^B$	0.29	-0.74	–
(iii)	$C_d = \min\left[(|\widetilde{\boldsymbol{u}}|/A)^B, C_{d,max}\right]$	0.22	$-2/3$	0.8
		0.38	-1	0.8
		0.48	$-4/3$	0.8

Table 2 Notations used to distinguish different treatments of the streamwise mean pressure gradient, where $U = \langle|\widetilde{\boldsymbol{u}}|\widetilde{\boldsymbol{u}}\rangle^{1/2}$ is the velocity scale associated with the total kinetic energy

Treatment of the streamwise mean pressure gradient	Mean canopy drag	Initial guess of drag coefficients
$\frac{1}{\rho_0}\frac{\partial\langle p\rangle}{\partial x}$, evaluated from (8)	$\langle f_x\rangle = \frac{\partial\langle u''w''\rangle}{\partial z} + \frac{1}{\rho_0}\frac{\partial\langle p\rangle}{\partial x}$	$C_{d,0} = \langle f_x\rangle/(aU^2)$
$\left[\frac{1}{\rho_0}\frac{\partial\langle p\rangle}{\partial x}\right]^{\text{fit}}$, fitted using (10)	$\langle f_x\rangle^{\text{fit}} = \frac{\partial\langle u''w''\rangle}{\partial z} + \left[\frac{1}{\rho_0}\frac{\partial\langle p\rangle}{\partial x}\right]^{\text{fit}}$	$C_{d,0}^{\text{fit}} = \langle f_x\rangle^{\text{fit}}/(aU^2)$
Neglected	$\langle f_x\rangle^\star = \frac{\partial\langle u''w''\rangle}{\partial z}$	$C_{d,0}^\star = \langle f_x\rangle^\star/(aU^2)$

to balance the divergence of the mean shear stress above the canopy (8), and it is the same as the imposed streamwise mean pressure gradient that drives the flow. Symbols with the superscript "fit" represent results for which the streamwise mean pressure gradient was fitted by applying (10) to values of $\langle C_d\rangle^\star_{\text{mod}} = -\gamma\left(\partial\langle u''w''\rangle/\partial z\right)$ and $\gamma = 1/\left(aU^2\right)$ below the location of the maximum $\langle C_d\rangle^\star_{\text{mod}}$ (see Sect. 2.2). Note that the mean shear stress consists of both resolved and SGS components, whereas the velocity scale associated with total kinetic energy (U) is obtained using the resolved velocity field only. Symbols with a superscript "$\star$" represent results for which the streamwise mean pressure gradient is neglected. Relevant symbols and notations are summarized in Table 2.

3.2 Initial Guess, Identification of Cases and Application of Iterative Approaches

Figures 2a, 3a, 4a, d, g show vertical profiles of the initial guess of drag coefficients ($C_{d,0}$, $C_{d,0}^{\text{fit}}$ and $C_{d,0}^\star$ defined in Table 2). Comparison between the estimators $C_{d,0}$ and $C_{d,0}^\star$ (*black plus signs* compared with *blue circles*; *green plus signs* compared with *magenta circles*) suggests that the streamwise mean pressure gradient is only negligible within the upper 1/3 of the canopy. Nevertheless, the behaviour of $C_{d,0}^\star$ at a given height suggests whether the drag coefficient is velocity dependent or not. When conditions change from high to low wind speeds (*blue and magenta circles*, respectively), the estimator $C_{d,0}^\star$ at a given height only remains constant for the case of a constant drag coefficient. For the cases of velocity-dependent drag coefficients (*circles* in Figs. 3a, 4a, d, g), a maximum in the profile of $C_{d,0}^\star$ is observed within the upper half of the canopy. Below the location of the maximum $C_{d,0}^\star$, changing the wind speed ($u_\star$) does not always yield consistent changes in $C_{d,0}$ and $C_{d,0}^\star$. Specifically, the modified characteristic velocity scale (U) at a given height increases with the imposed wind speed (characterized by $u_\star$). Consequently, at a given height in Figs. 3a, 4a, d, g, $C_{d,0}$ always decreases with increasing $u_\star$ (comparing *black and green plus signs*), whereas $C_{d,0}^\star$
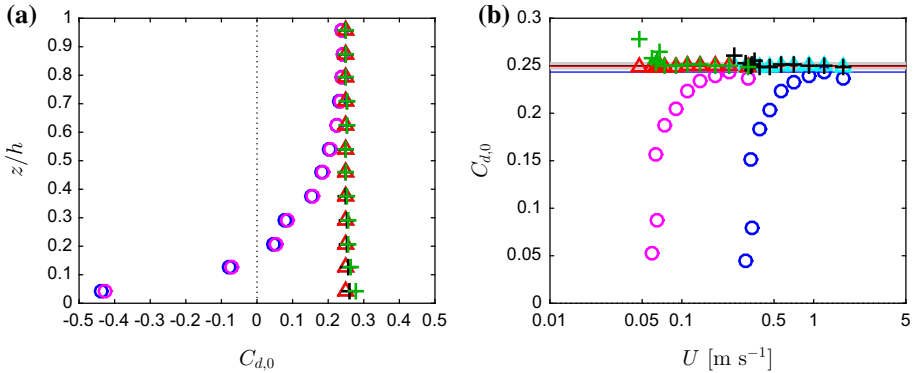
Fig. 2 Comparison of $C_{d,0}$ (*plus signs*), $C_{d,0}^{fit}$ (*triangles*) and $C_{d,0}^{\star}$ (*circles*) estimated for the case of a constant drag coefficient ($C_d = \langle C_d \rangle_{mod} = 0.25$). Estimators of drag coefficients are demonstrated against **a** height normalized by canopy height (z/h) and **b** the characteristic velocity scale ($U = \langle |\tilde{u}| \tilde{u} \rangle^{1/2}$). Results are shown for the strong ($u_{\star} = 0.51\,\mathrm{m\,s^{-1}}$; *black plus signs, blue circles and cyan triangles*) and weak ($u_{\star} = 0.1\,\mathrm{m\,s^{-1}}$; *green plus signs, magenta circles and red triangles*) wind cases. *Grey, black, red and blue solid lines* in **b** represent the model $\langle C_d \rangle_{mod} = \langle C_d \rangle_{mod}(U)$ imposed into LES and estimated from $C_{d,0}$, $C_{d,0}^{fit}$ and $C_{d,0}^{\star}$, respectively. For this case, these lines overlap
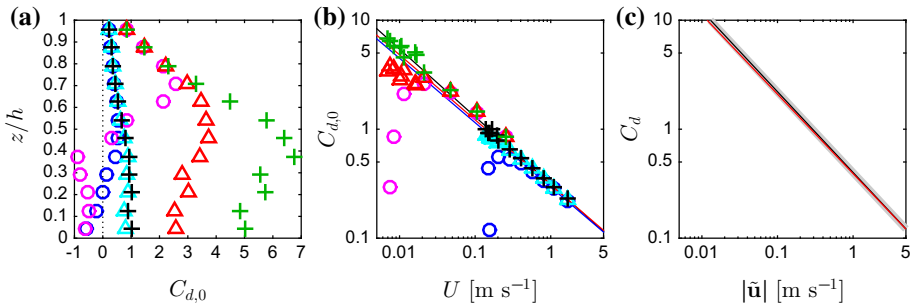

Fig. 3 Comparison of the drag coefficients estimated for the case of a power-law drag coefficient model ($C_d = (|\tilde{u}|/A)^B$, $A = 0.29\,\mathrm{m\,s^{-1}}$, $B = -0.74$). The estimators $C_{d,0}$, $C_{d,0}^{fit}$ and $C_{d,0}^{\star}$ are demonstrated against **a** height normalized by canopy height (z/h) and *b* the characteristic velocity scale ($U = \langle |\tilde{u}| \tilde{u} \rangle^{1/2}$). See Fig. 2 for representation of symbols. *Black, red and blue solid lines* in **b** represent the model $\langle C_d \rangle_{mod} = \langle C_d \rangle_{mod}(U)$ estimated from $C_{d,0}$, $C_{d,0}^{fit}$ and $C_{d,0}^{\star}$, respectively. In **c** the models of the instantaneous drag coefficient ($C_d = C_d(|\tilde{u}|)$) obtained using $\langle f_x \rangle$ and $\langle f_x \rangle^{fit}$ (*black and red lines*, respectively) are compared with the model imposed into LES (*grey line*)

can either increase or decrease with increasing $u_{\star}$ (comparing *blue and magenta circles*). In other words, if the streamwise mean pressure gradient is neglected, the data obtained below the location of the maximum $C_{d,0}^{\star}$ can provide misleading information about the drag–wind relationship.

The streamwise mean pressure gradient can be fitted by applying (10) to values of $\langle C_d \rangle_{mod}^{\star} = C_{d,0}^{\star}$ and $\gamma = 1/(aU^2)$ obtained below the location of the maximum $C_{d,0}^{\star}$. Using the fitted pressure gradient, the estimated drag coefficients $C_{d,0}^{fit}$ reproduce the behaviour of $C_{d,0}$. Note that $C_{d,0}$ characterizes the relationship between mean canopy drag and the local velocity scale U (*cyan triangles* compared with *black plus signs*; *red triangles* compared with *green plus signs*), showing that the new approach to estimate the mean pressure gradient
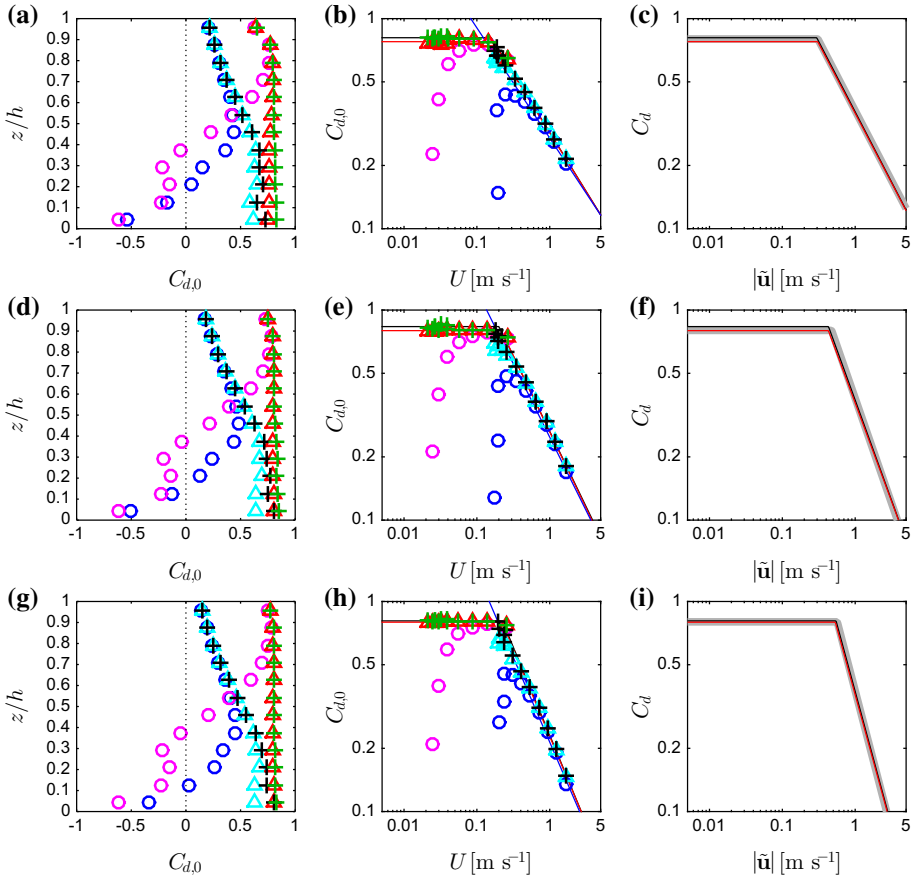
Fig. 4 Comparison of the drag coefficients estimated for the case of a capped power-law drag coefficient model $(C_d = \min\left((|\widetilde{\boldsymbol{u}}|/A)^B, C_{d,\max}\right), C_{d,\max} = 0.8)$. Simulations were conducted using three sets of parameters: **a–c** $A = 0.22\,\mathrm{m\,s^{-1}}$, $B = -2/3$; **d–f** $A = 0.38\,\mathrm{m\,s^{-1}}$, $B = -1$; **g–i** $A = 0.48\,\mathrm{m\,s^{-1}}$, $B = -4/3$. The estimators $C_{d,0}$, $C_{d,0}^{\mathrm{fit}}$ and $C_{d,0}^{\star}$ are demonstrated against **a, d, g** height normalized by canopy height (z/h) and **b, e, h** the characteristic velocity scale $(U = \langle|\widetilde{\boldsymbol{u}}|\widetilde{\boldsymbol{u}}\rangle^{1/2})$. See Fig. 2 for representation of symbols. *Black, red, and blue solid lines* in **b, e, h** represent the model $\langle C_d\rangle_{\mathrm{mod}} = \langle C_d\rangle_{\mathrm{mod}}(U)$ estimated from $C_{d,0}$, $C_{d,0}^{\mathrm{fit}}$ and $C_{d,0}^{\star}$, respectively. In **c, f, i** the models of the instantaneous drag coefficient $(C_d = C_d(|\widetilde{\boldsymbol{u}}|))$ obtained using $\langle f_x\rangle$ and $\langle f_x\rangle^{\mathrm{fit}}$ (*black and red lines*, respectively) are compared with the model imposed into LES (*grey lines*)

presented in Sect. 2.2 is practical and reliable. The only exception is the underestimation of $C_{d,0}$ by approximately 50 % in the lower half of the canopy for the case of a power-law drag coefficient model under weak wind conditions (*red circles* compared with *green plus signs* in Fig. 3a).

Although the estimator $C_{d,0} = \langle C_d\rangle_{\mathrm{mod}}$ does not quantify the correlation between instantaneous drag coefficients and instantaneous velocity, the dependence of $C_{d,0}$ on $U = \langle|\widetilde{\boldsymbol{u}}|\widetilde{\boldsymbol{u}}\rangle^{1/2}$ is clear. Over the investigated range of U, $C_{d,0} = C_{d,0}(U)$ shares the same functional form as the imposed model for the instantaneous drag coefficient $(C_d = C_d(|\widetilde{\boldsymbol{u}}|))$ (*plus signs* show a constant in Fig. 2b, a power law of U in Fig. 3b, and a capped power law of U in Fig. 4b,

e, h). As mentioned in Sect. 2.3, the specific functional form must be identified before the application of the iterative approaches presented in Sects. 2.3.1 and 2.3.2. Similar features are observed for the estimator $C_{d,0}^{fit}$ (*triangles* in Figs. 2b, 3b, 4b, e, h), which again confirms that the fitted streamwise mean pressure gradient is satisfactory.

Applying the iterative approaches to $\langle f_x \rangle$ reproduces the models of instantaneous drag coefficients imposed into LES (*black lines* compared with *grey lines* in Fig. 3c, 4b, f, i), confirming the applicability of the algorithms proposed in Sects. 2.3.1 and 2.3.2. Applying the iterative approaches to $\langle f_x \rangle^{fit}$ also reproduces the models imposed into LES for all cases (*red lines* compared with *grey lines* in Fig. 3c, 4b, f, i), which again confirms that the fitted streamwise mean pressure gradient is satisfactory. In conclusion, the approach of estimating the mean pressure gradient using (10) and then using an iterative method with a least-square fit is capable of recovering the instantaneous drag–wind relationship imposed in the LES.

4 Discussion

4.1 Implications for the Models of Mean Drag–Wind Relationships

Results in Sect. 3.2 show that the dependence of the modified mean drag coefficient on the velocity scale associated with total kinetic energy ($\langle C_d \rangle_{mod} = \langle C_d \rangle_{mod}(U)$) and the dependence of the instantaneous drag coefficient on the instantaneous velocity ($C_d = C_d(|\widetilde{\boldsymbol{u}}|)$) share the same functional form (*plus signs* in Figs. 2b, 3b, 4b, e, h compared with *grey solid lines* in Figs. 2b, 3c, 4c, f, i). Therefore the clear dependence of $\langle C_d \rangle_{mod}$ on U reported by field experimental studies (Cescatti and Marcolla 2004; Queck et al. 2012) supports the modelling approach that the instantaneous drag coefficient is described as a function of the instantaneous velocity. So far as the estimates of the streamwise mean pressure gradient are satisfactory, fitting the model $\langle C_d \rangle_{mod} = \langle C_d \rangle_{mod}(U)$ is trivial for all cases investigated in Sect. 3.2 (*black and red lines* fitted for *plus signs and triangles* in Figs. 2b, 3b, 4b, e, h). However, when the streamwise mean pressure gradient is neglected, the relationship between $\langle C_d \rangle_{mod}^{\star}$ and U obtained below the location of the maximum $\langle C_d \rangle_{mod}^{\star}$ does not always represent the relationship between $\langle C_d \rangle_{mod}$ and U. The practical procedure to determine whether the local drag coefficient is velocity-dependent is to investigate the estimator $\langle C_d \rangle_{mod}^{\star}$ for a given layer over a range of wind conditions. If the estimator $\langle C_d \rangle_{mod}^{\star}$ for a given layer remains constant over a range of wind speeds, then $\langle C_d \rangle_{mod}$ is a constant. If the constant $\langle C_d \rangle_{mod}$ does not vary with height, then the maximum of $\langle C_d \rangle_{mod}^{\star}$ at the canopy top can be used to approximate the value of $\langle C_d \rangle_{mod}$ (*blue line* compared with *grey line* in Fig. 2b). If the estimator $\langle C_d \rangle_{mod}^{\star}$ for a given layer varies with wind speeds, then $\langle C_d \rangle_{mod}$ depends on velocity. The dependence of $\langle C_d \rangle_{mod}$ on U can be inferred from the variability in $\langle C_d \rangle_{mod}^{\star}$ above the location of the maximum $\langle C_d \rangle_{mod}^{\star}$. For example, power-law functions of U can be fitted using $\langle C_d \rangle_{mod}^{\star}$ above the location of it maximum (*blue lines* in Fig. 3b, 4b, e, h).

One-dimensional and RANS models employ (3), for which a good model of $\langle C_d \rangle$ is required. Combining the streamwise components of (3) and (4) yields,

$$\frac{\langle C_d \rangle}{\langle C_d \rangle_{mod}} = \frac{\langle |\boldsymbol{u}|u \rangle}{\langle \boldsymbol{u} \rangle^2} \approx 1 + \frac{\langle u''u'' + (1/2)v''v'' + (1/2)w''w'' \rangle}{\langle u \rangle^2}, \qquad (21)$$

where the approximation in (21) is valid for $\left(v''v'' + w''w'' \right) / \left(\langle u \rangle \langle u \rangle + u''u'' \right) \ll 1$. Rewriting (21) provides a model for $\langle C_d \rangle$,

$$\langle C_d \rangle = (1 + F_{var}) \langle C_d \rangle_{mod}, \qquad (22)$$
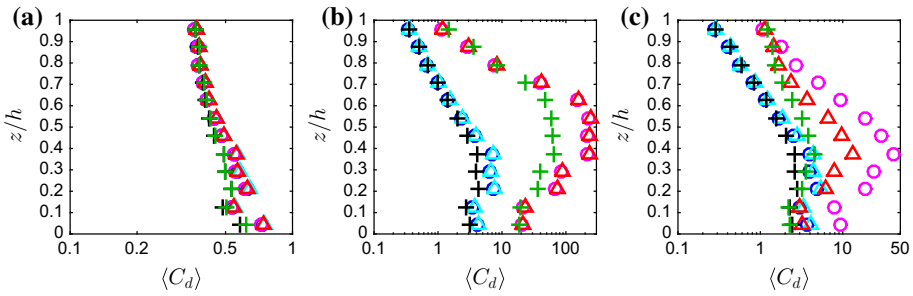
Fig. 5 The mean drag coefficient ($\langle C_d \rangle$) against normalized height (z/h) obtained for cases of the instantaneous drag coefficient being **a** a constant ($C_d = 0.25$), **b** a power-law function of velocity ($C_d = (|\tilde{u}|/A)^B$, $A = 0.29\ \mathrm{m\,s^{-1}}$, $B = -0.74$) and **c** a capped power-law function of velocity ($C_d = \min\left((|\tilde{u}|/A)^B, C_{d,\max}\right)$, $C_{d,\max} = 0.8$, $A = 0.38\ \mathrm{m\,s^{-1}}$, $B = -1$). Results of $\langle C_d \rangle$ were calculated using (3) (*plus signs*) and modeled using (22), where the models for the modified mean drag coefficient $\langle C_d \rangle_{\mathrm{mod}} = \langle C_d \rangle_{\mathrm{mod}}(U)$ are fitted $C_{d,0}^{\mathrm{fit}}$ and $C_{d,0}^{\star}$ (*circles and triangles, respectively*). Results are shown for the strong ($u_\star = 0.51\ \mathrm{m\,s^{-1}}$; *black plus signs, blue circles and cyan triangles*) and weak ($u_\star = 0.1\ \mathrm{m\,s^{-1}}$; *green plus signs, magenta circles and red triangles*) wind cases. For the case of $C_d = \min\left((|\tilde{u}|/A)^B, C_{d,\max}\right)$, results are only shown for the case of $A = 0.38\ \mathrm{m\,s^{-1}}$ and $B = -1$, because results for the other two cases show similar pattern and suggest the same conclusion

where $F_{\mathrm{var}} = \langle u''u'' + (1/2)v''v'' + (1/2)w''w'' \rangle / \langle u \rangle^2$ measures the relative importance of the variances of velocity fluctuations (i.e., components of TKE and DKE) and the kinetic energy of the mean flow. The variances of velocity components affect $\langle C_d \rangle$ in both the multiplier $(1 + F_{\mathrm{var}})$ before $\langle C_d \rangle_{\mathrm{mod}}$ and the effective velocity ($U = \langle |u|u \rangle^{1/2} \approx (1 + F_{\mathrm{var}}) \langle u \rangle$) in the model of $\langle C_d \rangle_{\mathrm{mod}}$. In general, the effects of TKE and DKE are most profound in the lower canopy region, where the values of $\langle C_d \rangle$ can be greater than twice the values of $\langle C_d \rangle_{\mathrm{mod}}$ (*plus signs* in Fig. 5 compared with *plus signs* in Figs. 2a, 3a, 4d). The functional form (22) represents a feedback mechanism between the variances of velocity components and the mean drag–wind relationship, and can be easily implemented into canopy-resolving one-dimensional and RANS models that use second- and higher-order closure schemes for turbulence. With a reasonable approximation, $F_{\mathrm{var}} \approx \langle u''u'' + v''v'' + w''w'' \rangle / \langle u \rangle^2 = 2(\mathrm{TKE} + \mathrm{DKE})/\langle u \rangle^2$, the functional form (22) can be implemented into 1.5-order closure models as well.

For the case of a constant instantaneous drag coefficient ($C_d = \langle C_d \rangle_{\mathrm{mod}}$), $\langle C_d \rangle$ generally increases with decreasing distance to the ground (*plus signs* in Fig. 5a), consistent with the trend reported for rigid canopies (Poggi et al. 2004b; Santiago et al. 2008). As suggested by DNS results of Santiago et al. (2008), the instantaneous drag coefficient (C_d) for a canopy of rigid cubes is approximately a constant, and most of the variability in the mean drag coefficient ($\langle C_d \rangle$) is attributed to the contribution from the components of TKE and DKE. Removing the variability in $\langle C_d \rangle$ caused by variability in *TKE* and *DKE* is critical for investigating the drag–wind relationships.

For the cases of velocity-dependent instantaneous drag coefficient, plugging the model of $\langle C_d \rangle_{\mathrm{mod}}(U)$ fitted using $C_{d,0}^{\mathrm{fit}}$ and U (*red lines* in Figs. 2b, Figs. 3b, 4b, e, h) into (22) yields good estimates of $\langle C_d \rangle$ in general (*cyan and red triangles* compared with *black and green plus signs* in Fig. 5, respectively). However, $\langle C_d \rangle$ in the mid-canopy region ($0.2 < z/h < 0.6$) can be overestimated by 300 % for the weak wind cases (*red triangles* compared with *green plus signs* in Figs. 5b, c). Inserting the model of $\langle C_d \rangle_{\mathrm{mod}}(U)$ fitted using $C_{d,0}^{\star}$ and U above the

location of the maximum $C_{d,0}^{\star}$ (*blue lines* in in Figs. 2b, 3b, 4b, e, h) into (22) provides similar results of $\langle C_d \rangle$, except for the weak wind cases of a capped power-law drag coefficient (*blue and magenta circles* compared with *cyan and red triangles* in Fig. 5, respectively). For this specific case $\langle C_d \rangle$ in the lower 2/3 of the canopy is overestimated by an order of magnitude (*magenta circles* compared with *green plus signs* in Fig. 4c), because the power law fitted using $\langle C_d \rangle_{mod}^{\star}$ above the location of its maximum does not capture the behaviour of $\langle C_d \rangle_{mod}$ under low wind conditions.

4.2 Implications for the Displacement Height

The displacement height is defined for a virtual wall boundary layer that reproduces flow statistics above the canopy roughness sublayer. The definition given by Jackson (1981) aimed at reproducing the total mean shear stress within and above the canopy. Specifically, the profile of mean shear stress above the canopy remains unchanged, and it is extrapolated below the canopy top to provide the mean shear stress for the virtual wall boundary layer. The displacement height is linked to the penetration thickness of the mean shear stress,

$$d_0 = h - \frac{\int_0^h \langle u''w'' \rangle \mathrm{d}z}{\langle u''w'' \rangle_{z/h=1} + \left(\frac{h-d_0}{2} \right) \frac{1}{\rho_0} \frac{\partial \langle p \rangle}{\partial x}}, \tag{23}$$

where $\left(\int_0^h \langle u''w'' \rangle \mathrm{d}z \right)$ is the total mean shear stress within the canopy, and $\left(\langle u''w'' \rangle_{z/h=1} + [(h - d_0)/2](1/\rho_0)(\partial \langle p \rangle/\partial x) \right)$ is the average virtual mean shear stress between the virtual wall and the canopy top. Note that (23) is more general than the expression used by Jackson (1981), which assumed a zero streamwise mean pressure gradient and that the mean shear stress does not penetrate to the ground beneath the canopy. If the term associated with the streamwise mean pressure gradient is removed from (23), then the distance between the virtual wall and the canopy top $(h - d_0)$ is a fraction of the canopy layer determined by the canopy-averaged mean shear stress and the canopy-top shear stress (Sogachev and Kelly 2015). With this simplification, (23) becomes,

$$d_0 = \frac{\int_0^h z \frac{\partial \langle u''w'' \rangle}{\partial z} \mathrm{d}z}{\langle u''w'' \rangle_{z/h=1}}, \tag{24}$$

where the relationship $h \langle u''w'' \rangle_{z/h=1} = \int_0^h \left[(z \langle u''w'' \rangle)/\partial z \right] \mathrm{d}z$ is employed. Scale analysis suggests that replacing (23) with (24) induces less than 1 % difference in d_0 if the boundary-layer thickness is an order of magnitude greater than the canopy height. Compared with the definition of displacement height based on other flow statistics (e.g., the mean wind), this definition based on the mean shear stress has two major advantages: (i) the mean shear stress is the fundamental flow statistic that determines the characteristic velocity scale for turbulent shear flows above solid boundaries, and (ii) the profile of the mean shear stress above the canopy is uniquely determined by the boundary-layer thickness and the streamwise mean pressure gradient. Therefore we adopt the definition of displacement height proposed by Jackson (1981), requiring the virtual wall boundary layer to reproduce the total mean shear stress within and above the canopy. Comparing *plus signs* with *circles* in Fig. 6a confirms that (23) and (24) produce approximately the same estimates of the displacement height. For the case of a constant drag coefficient (*black symbols* compared with *green symbols* in Fig. 6a), the estimates of d_0 do not vary with wind conditions. For the cases of velocity-dependent drag coefficients (*red and magenta symbols* compared with *blue and cyan symbols* in Fig. 6a), the estimates of d_0 increase by 10–16 % when the friction velocity $(u_\star)$ decreases from $0.5 \, \mathrm{m \, s^{-1}}$
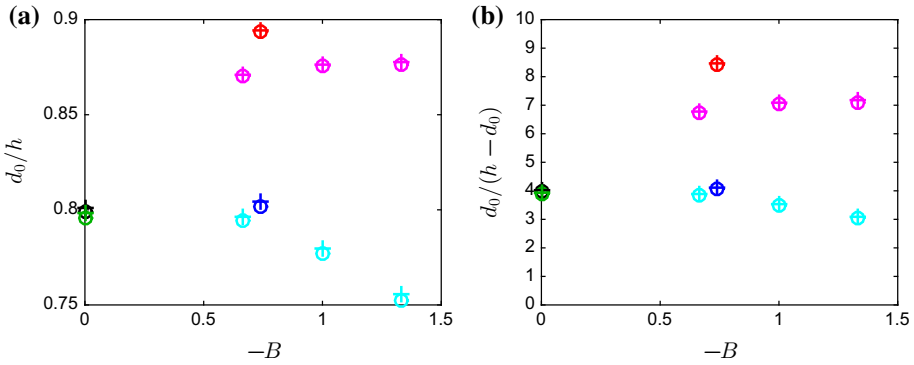
Fig. 6 **a** The displacement height normalized by canopy height (d_0/h) and **b** the multiplier ($d_0/(h - d_0)$) estimated using (23; *plus signs*) and (24; *circles*) against the power-law exponent (B). Results are shown for the strong ($u_\star = 0.51\,\mathrm{m\,s^{-1}}$; *black, blue and cyan symbols*) and weak ($u_\star = 0.1\,\mathrm{m\,s^{-1}}$; *green, red and magenta symbols*) wind cases and for three cases of drag coefficient models investigated in Sect. 3: a constant ($B = 0$; *black and green symbols*), a power-law function of velocity ($B = -0.74$; *blue and red symbols*) and a capped power-law function of velocity ($B = -2/3, -1$ and $-4/3$; *cyan and magenta symbols*)

to $0.1\,\mathrm{m\,s^{-1}}$. As a reference, a 6 % increase in d_0 was reported for a bean canopy by Thom (1971), when $u_\star$ decreased from 0.35 to $0.19\,\mathrm{m\,s^{-1}}$.

Assuming a smooth transition from an exponential to a logarithmic mean wind profile at the canopy top, Seginer (1974) proposed a proportionality between the roughness length and the distance between the virtual wall and the canopy top, $z_0 = \lambda(h - d_0)$. Although the assumption used by Seginer (1974) is violated by the presence of the canopy roughness sublayer, laboratory and field experimental studies (Thom 1971; Legg and Long 1975; Hicks et al. 1975) reported the evidence of the proportional relationship between z_0 and $(h - d_0)$. This empirical relationship implies that the variability in the roughness length ($\Delta z_0/z_0$) corresponds to the variability in the displacement height ($\Delta d_0/d_0$) multiplied by ($-d_0/(h - d_0)$). Fig. 6b shows that the absolute value of this multiplier ranges from 3 to 9, implying that the 10–16 % increase in the displacement height leads to a more than 30 % decrease in the roughness length.

5 Summary

We have explored practical approaches for estimating the streamwise mean pressure gradient and models for the instantaneous local drag coefficients that require no additional input data with respect to traditional approaches. As described in Sect. 2, the traditional and revised approaches share the same assumptions: (i) the canopy is homogeneous and infinite in both horizontal directions; (ii) the temperature stratification within the canopy is homogeneous in the horizontal; (iii) the flow is in a statistically steady state; (iv) spatially-averaged metrics for the flow are available; (v) the vertical distribution of leaf area density is known; and (vi) the instantaneous drag coefficient is modelled as an analytical function of the instantaneous velocity. These assumptions are satisfied by the LES data used to validate the revised approaches.

Compared with the traditional approaches, the new approaches require additional procedures of data analysis. Firstly, a least-square fitting was proposed to provide estimates of

the streamwise mean pressure gradient. Traditionally, reliable estimates of the streamwise mean pressure gradients are unavailable for terrestrial field experiments, and therefore estimates of the mean canopy drag are only reliable within the upper canopy region. When the streamwise mean pressure gradient is neglected, the estimates of the modified local mean drag coefficient, $\langle C_d \rangle^\star_{\text{mod}}$, only describes the component of mean drag that balances the vertical gradient of mean vertical momentum flux. The variability in $\langle C_d \rangle^\star_{\text{mod}}$ for a given layer indicates whether the instantaneous drag coefficient is velocity-dependent or not. However, the relationship between $\langle C_d \rangle^\star_{\text{mod}}$ and $U = \langle |\boldsymbol{u}|u \rangle^{1/2}$ below the location of the maximum of $\langle C_d \rangle^\star_{\text{mod}}$ does not reflect the dependence of $\langle C_d \rangle_{\text{mod}}$ on U. Using the fitted streamwise mean pressure gradient, reliable estimates for the mean canopy drag can be made within the entire canopy layer, including the lower canopy region, and the dependence of $\langle C_d \rangle_{\text{mod}}$ on U is reproduced. As far as an analytical model can be used to describe the dependence of the modified mean drag coefficient ($\langle C_d \rangle_{\text{mod}}$) on the characteristic velocity scale (U), the same functional form can be used to describe the dependence of the instantaneous drag coefficient (C_d) on instantaneous velocity ($\boldsymbol{u}$). Secondly, iterative approaches were proposed for specific cases to estimate the instantaneous drag coefficient as a function of instantaneous velocity, which was not quantified by traditional approaches. Validation against LES results showed that these approaches reproduced the models of the instantaneous drag coefficient imposed into LES.

The local mean drag coefficient ($\langle C_d \rangle$) depends on both the mean velocity and the variances of velocity components, and accounting for the contribution from velocity variances is critical for investigating and modelling the relationship between mean drag and mean velocity. Using $\langle C_d \rangle_{\text{mod}} = \langle C_d \rangle_{\text{mod}}(U)$ obtained from $C^{\text{fit}}_{d,0}$ provided satisfactory estimates of $\langle C_d \rangle$ in general. For cases of the velocity-dependent instantaneous drag coefficient, the displacement height increased by 10–16 % when the friction velocity decreased from 0.5 to $0.1\,\text{m\,s}^{-1}$, corresponding to more than 30 % decrease in the roughness length. Quantifying the variability in the roughness length is essential for models that parametrize the canopy layer as a rough-wall boundary condition.

Both the traditional and new approaches require input data of spatially-averaged metrics of statistically stationary flow within and above horizontally homogeneous canopy, which are typically unavailable for laboratory and field experiments. Thus applying these approaches to single-point observational data requires the quantification of instrumental errors and the investigation of data representativeness.

References

Albayrak I, Nikora V, Miler O, OHare M (2012) Flow-plant interactions at a leaf scale: effects of leaf shape, serration, roughness and flexural rigidity. Aquat Sci 74:267–286

Alben S, Shelley M, Zhang J (2002) Drag reduction through self-similar bending of a flexible body. Nature 420:479–481

Baldocchi D, Meyers TP (1998) Turbulence structure in a deciduous forest. Boundary-Layer Meteorol 43:345–364

Bou-Zeid E, Meneveau C, Parlange MB (2005) A scale-dependent Lagrangian dynamic model for large eddy simulation of complex turbulent flows. Phys Fluids 17:025105. doi:10.1063/1.1839152

Cescatti A, Marcolla B (2004) Drag coefficient and turbulence intensity in conifer canopies. Agric For Meteorol 121:197–206

Dupont S, Brunet Y, Jarosz N (2006) Eulerian modelling of pollen dispersal over heterogeneous vegetation canopies. Agric For Meteorol 141:82–104

Dupont S, Brunet Y (2008) Influence of foliar density profile on canopy flow: a large-eddy simulation study. Agric For Meteorol 148:976–990

Gavrilov K, Morvan D, Accary G, Lyubimov D, Meradji S (2013) Numerical simulation of coherent turbulent structures and of passive scalar dispersion in a canopy sublayer. Comput Fluids 78:54–62

Gaylord B, Blanchette CA, Denny MW (1994) Mechanical consequences of size in wave-swept algae. Ecol Monogr 64:287–313

Ghisalberti M, Nepf H (2004) The limited growth of vegetated shear layers. Water Resour Res 40:W07,502

Gleicher SC, Chamecki M, Isard SA, Pan Y, Katul GG (2014) Interpreting three-dimensional spore concentration measurements and escape fraction in a crop canopy using a coupled Eulerian–Lagrangian Stochastic model. Agric For Meteorol 194:118–131

Gosselin F, de Langre E, Machado-Almeida B (2010) Drag reduction of flexible plates by reconfiguration. J Fluid Mech 650:319–341

Harder DL, Speck O, Hurd CL, Speck T (2004) Reconfiguration as a prerequisite for survival in highly unstable flow-dominated habitats. J Plant Growth Regul 23:98–107

Hicks BB, Hyson P, Moore CJ (1975) A study of eddy fluxes over a forest. J Appl Meteorol 14:58–66

Jackson PS (1981) On the displacement height in the logarithmic velocity profile. J Fluid Mech 111:15–25

Katul GG (1998) An investigation of higher-order closure models for a forested canopy. Boundary-Layer Meteorol 89:47–74

Katul GG, Grönholm T, Launiainen S, Vesala T (2011) The effects of the canopy medium on dry deposition velocities of aerosol particles in the canopy sub-layer above forested ecosystems. Atmos Environ 45:1203–1212

Legg BJ, Long IF (1975) Turbulent diffusion within a wheat canopy: II. Results and interpretation. Q J R Meteorol Soc 101:611–628

Luhar M, Nepf HM (2011) Flow-induced reconfiguration of buoyant and flexible aquatic vegetation. Limnol Oceanogr 56:2003–2017

Pan Y, Chamecki M, Isard SA (2014a) Large-eddy simulation of turbulence and paticle dispersion inside the canopy roughness sublayer. J Fluid Mech 753:499–534

Pan Y, Follett E, Chamecki M, Nepf H (2014b) Strong and weak, unsteady reconfiguration and its impact on turbulence structure within plant canopies. Phys Fluids 26:105,102

Patton EG, Sullivan PP, Davis KJ (2003) The influence of a forest canopy on top-down and bottom-up diffusion in the planetary boundary layer. Q J R Meteorol Soc 129:1415–1434

Pinard JDJP, Wilson JD (2001) First-and second-order closure models for wind in a plant canopy. J Appl Meteorol 40:1762–1768

Poggi D, Katul GG, Albertson JD (2004a) Momentum transfer and turbulent kinetic energy budgets within a dense model canopy. Boundary-Layer Meteorol 111:589–614

Poggi D, Porporato A, Ridolfi L, Albertson JD, Katul GG (2004b) The effect of vegetation density on canopy sub-layer turbulence. Boundary-Layer Meteorol 111:565–587

Queck R, Bienert A, Maas HG, Harmansa S, Goldberg V, Bernhofer C (2012) Wind fields in heterogeneous conifer canopies: parameterisation of momentum absorption using high-resolution 3D vegetation scans. Eur J For Res 131:165–176

Raupach MR, Shaw RH (1982) Averaging procedures for flow within vegetation canopies. Boundary-Layer Meteorol 22:79–90

Raupach MR, Thom AS (1981) Turbulence in and above plant canopies. Annu Rev Fluid Mech 13:97–129

Santiago JL, Coceal O, Martilli A, Belcher SE (2008) Variation of the sectional drag coefficient of a group of buildings with packing density. Boundary-Layer Meteorol 128:445–457

Schlichting H, Gersten K (2000) Boundary-layer theory. Springer, Berlin, 799 pp

Seginer I (1974) Aerodynamic roughness of vegetated surfaces. Boundary-Layer Meteorol 5:383–393

Shaw RH, Patton EG (2003) Canopy element influences on resolved-and subgrid-scale energy within a large-eddy simulation. Agric For Meteorol 115(1):5–17

Shaw RH, Schumann U (1992) Large-eddy simulation of turbulent flow above and within a forest. Boundary-Layer Meteorol 61:47–64

Sogachev A, Kelly M (2015) On displacement height, from classical to practical formulation: stress, turbulent transport and vorticity considerations. Boundary-Layer Meteorol. doi:10.1007/s10546-015-0093-x

Su HB, Shaw RH, Paw KT, Moeng CH, Sullivan PP (1998) Turbulent statistics of neutrally stratified flow within and above a sparse forest from large-eddy simulation and field observations. Boundary-Layer Meteorol 88:363–397

Thom AS (1971) Momentum absorption by vegetation. Q J R Meteorol Soc 97:414–428

Vogel S (1984) Drag and flexibility in sessile organisms. Am Zool 24:37–44

Wilson JD, Ward DP, Thurtell GW, Kidd GE (1982) Statistics of atmospheric turbulence within and above a corn canopy. Boundary-Layer Meteorol 24:495–519

Wilson JD (1988) A second-order closure model for flow through vegetation. Boundary-Layer Meteorol 42:371–392

Wilson NR, Shaw RH (1977) A higher order closure model for canopy flow. J Appl Meteorol 16:1197–1205

Yue W, Meneveau C, Parlange MB, Zhu W, Van Hout R, Katz J (2007a) A comparative quadrant analysis of turbulence in a plant canopy. Water Resour Res 43:W05,422

Yue W, Parlange MB, Meneveau C, Zhu W, Van Hout R, Katz J (2007b) Large-eddy simulation of plant canopy flows using plant-scale representation. Boundary-Layer Meteorol 124:183–203